11th Edition of the

International Conferences on
Wind Turbine Noise

Copenhagen, Denmark – 10th to 13th June 2025

Multi-Scale Turbulence Structures in Grid-Generated Turbulence for Leading Edge Noise Prediction

Sparsh Sharma[1], Alexandre Suryadi and Michaela Herr
German Aerospace Center (DLR), 38108 Braunschweig, Germany

Summary

This study investigates multi-scale turbulence characteristics and their impact on leading-edge noise generation in controlled wind tunnel conditions. Using a turbulence grid mounted in the Acoustic Wind Tunnel Braunschweig (AWB), the inflow turbulence is experimentally characterised and numerically reproduced via large eddy simulations (LES) in OpenFOAM. The analysis focuses on the spatial evolution of turbulence intensity, integral length scales, and energy spectra upstream and downstream of a NACA0012 airfoil. Comparisons between LES and experimental measurements show excellent agreement across key metrics, validating the simulation's fidelity. Vortical structure visualisation and spectral analysis reveal how turbulence decays, distorts, and regenerates through airfoil interaction. These flow dynamics are directly linked to the observed sound pressure level (SPL) spectra and far-field directivity patterns. The findings confirm that grid-generated turbulence drives leading-edge noise through coherent-structure interactions, consistent with classical theories and modern computational predictions.

1. Introduction

Leading-edge noise arises from the unsteady interaction between turbulent inflow structures and the leading edge of an airfoil. In wind energy applications, this mechanism is a major contributor to aeroacoustic emissions, affecting both operational efficiency and environmental compliance. Understanding and predicting leading-edge noise is therefore critical to improving rotor blade designs and reducing turbine noise footprints.

The theoretical basis for leading-edge noise was established by Amiet [1], who developed a semi-empirical model assuming homogeneous, isotropic turbulence interacting with an incompressible flat-plate airfoil. This formulation has been widely adopted in noise prediction frameworks. However, recent studies have shown that real-world turbulence—particularly in wind energy scenarios—is often anisotropic, intermittent, and structured across multiple scales [2, 3]. These deviations from idealised assumptions significantly impact noise generation and radiation characteristics.

To study airfoil–turbulence interaction under controlled and repeatable conditions, researchers frequently employ turbulence-generating grids in wind tunnel experiments. These grids produce defined turbulence intensities and length scales, allowing systematic investigation of how turbulence properties affect noise. Experimental studies consistently report that increased turbulence intensity raises overall noise levels, while larger integral length scales shift dominant noise frequencies to lower ranges [4, 5].

Complementing experimental approaches, high-fidelity numerical simulations—particularly large eddy

[1]Corresponding author - Email: sparsh.sharma@dlr.de

simulation (LES)—offer a powerful means of resolving the spatial and temporal evolution of turbulent structures. LES has demonstrated superior capability in reproducing flow dynamics and associated noise mechanisms compared to lower-fidelity methods. Recent work [6, 7] highlights the importance of capturing turbulence intermittency, anisotropy, and coherent structures to accurately model leading-edge noise.

Despite progress, several open questions remain regarding the predictive capability of numerical simulations for leading-edge noise. One key challenge is to assess how well LES-based simulations reproduce turbulence and noise characteristics when compared directly with experimental data. Additionally, it is important to understand how turbulence evolves as it convects from the grid towards and through the airfoil, and how this evolution influences noise generation mechanisms.

This study addresses these questions using a combined numerical and experimental approach. Controlled inflow turbulence is generated in the Acoustic Wind Tunnel Braunschweig (AWB) using a passive turbulence grid. A series of LES calculations are performed in OpenFOAM to reproduce the same setup, resolving turbulence evolution and airfoil interaction in detail. The analysis focuses on turbulence intensity, integral length scales, energy spectra, coherent structures, and acoustic radiation. By comparing LES predictions with hot-wire and microphone array measurements, we evaluate the fidelity of turbulence resolution and its acoustic relevance.

The remainder of this paper is structured as follows. Section 2 outlines the numerical methodology and computational setup used in the large eddy simulations (LES), while Section 3 describes the experimental configuration in the Acoustic Wind Tunnel Braunschweig (AWB). Section 4 presents a comparative analysis of turbulence intensity, integral length scales, vortical structures, velocity spectra, and far-field sound pressure levels obtained from both LES and experimental data. Finally, the conclusions are summarised in Section 5.

2. Numerical Setup

Large Eddy Simulation (LES) is used to model near-field turbulence, with a subgrid scale model (SGS) accounting for unresolved eddies, while larger scales are directly resolved. The governing equations are derived by spatial filtering of the incompressible Navier-Stokes equations, incorporating the Smagorinsky SGS model with a dimensionless time step of $\Delta t^* = 0.012$. The computational framework, numerical schemes, and boundary conditions closely follow our previous work [8], where further implementation details can be found.

The numerical domain is designed to replicate the AWB, with grid-generated turbulence introduced upstream of the airfoil. The three-dimensional computational domain extends six airfoil chord lengths ($6D$) upstream to the velocity inlet and 28 chord lengths ($28D$) downstream to the pressure outlet. The upper and lower boundaries are set as symmetry planes, located $3D$ away from the airfoil chord line. The NACA 0012 airfoil is modelled with a no-slip condition, while the turbulence grid is also treated as a solid boundary.

The freestream velocity in the simulations was initially varied as $U_\infty \in [20, 30, 40]$ m/s. However, in the present study, we focus exclusively on the case of $U_\infty = 20$ m/s. A refined mesh is applied near the airfoil to resolve the viscous sublayer, ensuring a dimensionless wall distance $y^+ < 1$. The spanwise direction is treated with periodic boundary conditions across 100 parallel planes spanning $4D$, enabling an efficient representation of the inflow turbulence. The computational grid consists of 80 million cells, ensuring adequate resolution of the turbulent structures.

Unlike the experimental setup, the numerical model omits the physical wind tunnel nozzle and its contraction ratio, as its primary focus is on simulating the airfoil-turbulence interaction.

3. Experimental Setup

The experimental investigations were carried out in the Acoustic Wind Tunnel Braunschweig (AWB) at DLR. The AWB is a closed-loop, anechoic open test section wind tunnel designed to minimise sound reflection above 200 Hz.

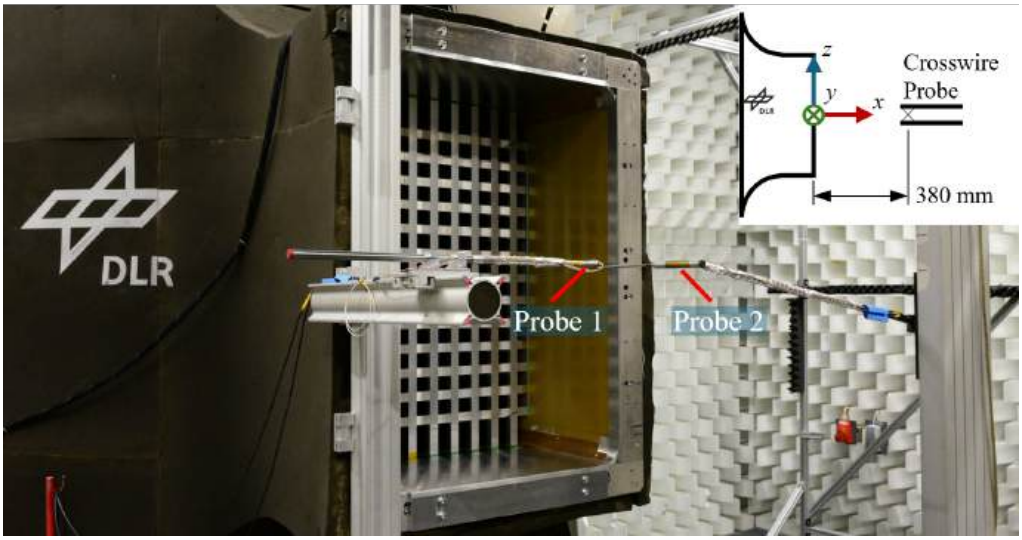

Figure 1 The AWB equipped with a turbulence grid and 2 cross-wire probes for flow measurements.

The wind tunnel operates at velocities up to 65 m/s, with a relatively low turbulence intensity of 0.3%. The flow is introduced into the test section through an 800 mm span and 1200 mm high rectangular nozzle, as shown in Fig. 1, along with the turbulence grid and two cross-wire velocity probes placed 380 mm downstream of the nozzle.

To produce varying inflow turbulence intensities, the AWB was equipped with a turbulence grid generator. The grid is made of rectangular profile bars with dimensions $d = 20$ mm and the distance between the bars is $M = 60$ mm. It should be noted that the maximum freestream velocity, U_∞, decreases to below 40 m/s as the blockage ratio exceeds 33%, limiting the Reynolds number range that can be studied. The grid is installed 495 mm upstream of the nozzle, 875 mm from the velocity probes, ensuring a minimum development distance of $10M$ for the turbulence to develop into isotropic turbulence.

The leading-edge noise was analysed using the coherent output power technique introduced by Brooks and Hodgson [9] and was applied for the investigation of leading-edge noise by Hutcheson and Brooks [10]. Two sets of line-array consisting of Bruel&Kjær microphones were installed with 6 1/4-inch microphones 746 mm above the model and 8 1/4-inch microphones 1244 mm below. After factoring refraction of sound by the test section's shear layer, the difference of the distance between the model's edge and the respective microphones was compensated for by delaying one of the two measured signals. The time delay was determined from the cross-correlation of two measurement signals from the microphones above and below the model. The predominant noise source position was determined by cross-correlating two microphones from either above or below the model. In this manner, the leading-edge noise will have a shorter path to the upstream microphone, and vis-a-vis, the trailing-edge noise will have shorter path to the downstream microphone. Namely, the leading-edge noise will have a time-lag and the trailing-edge noise a time-lead. It was with the turbulence grid generator, the predominant noise source is radiating from the leading edge position. The COP analysis produces a cross-spectrum and a phase-spectrum that is out-of-phase as a result of measuring the edge radiated noise at opposite directivity angles. If the conditions of out-of-phase spectrum and phase-lag cross-correlation are considered, the cross-spectral density is taken to be representative of the power spectral density of the leading-edge noise eliminating the incoherent noise sources inside the test section.

4. Results and Discussion

In this section, we analyse the turbulence characteristics from both numerical and experimental perspectives. The discussion follows a structured approach, beginning with turbulence intensity and integral length scales, followed by intermittency analysis, coherence decay, and energy spectra. The trends observed are compared

with previous research findings to highlight their significance.

4.1 Turbulence Intensity and Integral Length Scale

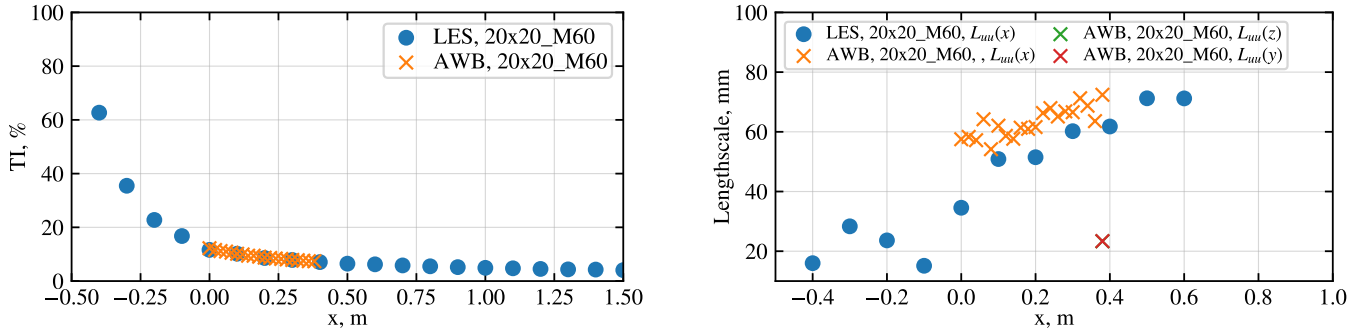

(a) *(b)*

Figure 2 (a) Turbulence intensity and (b) integral length scales at different locations in the streamwise direction for a NACA0012 airfoil at $U_\infty = 20$ m/s with a turbulence grid of $M = 60$ mm.

Figure 2a compares the decay of turbulence intensity (TI) predicted by LES (blue dots) with experimental AWB wind tunnel measurements (orange crosses). Turbulence intensity is defined as the ratio of the root-mean-square (RMS) of velocity fluctuations to the mean free-stream velocity:

$$\mathrm{TI} = \frac{\sqrt{\frac{1}{3}\left(\overline{u'^2} + \overline{v'^2} + \overline{w'^2}\right)}}{U_\infty}. \tag{1}$$

Here, u', v', and w' are the components of the instantaneous velocity fluctuations and U_∞ is the mean freestream velocity. Both datasets exhibit the expected power-law decay typical of grid-generated turbulence [11]. Immediately downstream of the grid ($x \approx -0.5$ m), turbulence intensities are highest, consistent with strong wake-induced turbulence reported by Liu et al. [12]. LES predictions closely align with experimental results near the airfoil leading edge ($x = 0$ m), indicating reliable modelling of turbulence dissipation processes crucial for aeroacoustic studies [13].

Further downstream ($x > 0$ m), the experimental TI values plateau slightly, reflecting open-jet effects such as ambient air entrainment, as also observed by Bowen et al. [14]. Conversely, LES continues a mild decay, suggesting boundary condition limitations or numerical dissipation in the far field [12]. Overall, the strong qualitative and quantitative agreement confirms the validity of the LES setup, aligning well with classical [15] and recent computational studies [13, 16], while highlighting minor aspects for simulation refinement.

Figure 2b compares the streamwise integral length scale $L_{uu}(x)$ derived from LES (blue dots) with experimental measurements (orange crosses) from the AWB wind tunnel. The integral length scale in the streamwise direction is defined based on the autocorrelation function $R_{uu}(r)$ of the velocity fluctuations u':

$$L_{uu}(x) = \int_0^\infty R_{uu}(r)\, dr, \quad \text{where} \quad R_{uu}(r) = \frac{\overline{u'(x,t)u'(x+r,t)}}{\overline{u'^2(x,t)}}. \tag{2}$$

Both datasets reveal a clear trend of increasing integral length scales downstream of the turbulence grid, indicating a progressive aggregation of turbulent structures as smaller eddies merge into larger coherent motions. This behaviour contrasts classical turbulence theories [17, 18], which typically predict monotonic decay of length scales due to continuous energy dissipation.

Recent literature increasingly supports this transient growth in integral length scales. Burton et al. [19] and Wang et al. [7] reported similar downstream growth, attributing it to vortex merging mechanisms transferring

energy to larger-scale structures. The excellent agreement between LES and experimental data near the airfoil ($x = 0\,\text{m}$) further validates the simulation's fidelity, consistent with high-quality LES validations presented by Trascinelli et al. [13].

Minor discrepancies between LES and experiments downstream ($x > 0.5\,\text{m}$) may arise from differences in boundary conditions, mesh resolution limitations, or numerical dissipation in LES [12]. Nonetheless, the overall consistency confirms that the LES reliably captures the dynamic evolution of turbulence structures, essential for accurate aeroacoustic predictions.

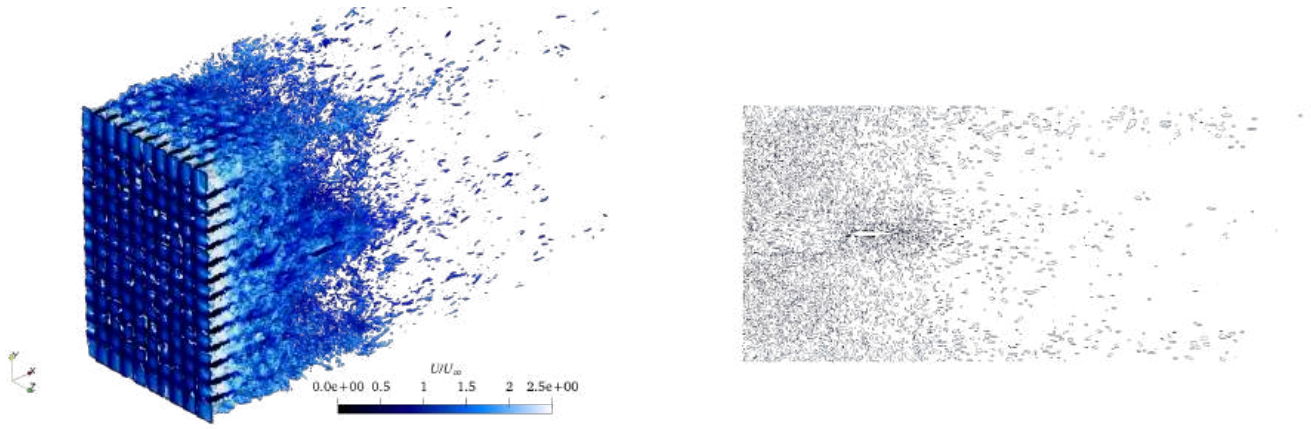

(a) *(b)*

Figure 3 (a) Isosurfaces of Q-criterion visualizing coherent vortical structures downstream of the M60 turbulence grid, coloured by instantaneous velocity magnitude and (b) streamwise-parallel slice of the instantaneous Q-criterion field taken at the mid-span $y/D = 0$.

Figure 3a visualises the vortical structures using the Q-criterion at the final simulation timestep for the M60 grid and freestream velocity of 20 m/s. The Q-criterion is defined as:

$$Q = \frac{1}{2}\left(\|\mathbf{\Omega}\|^2 - \|\mathbf{S}\|^2\right), \tag{3}$$

where $\mathbf{\Omega}$ is the asymmetric part of the velocity gradient tensor (vorticity tensor), and $\mathbf{S}$ is the symmetric part (rate-of-strain tensor). A positive Q value indicates regions where rotation dominates over strain, marking coherent vortex structures.

Immediately downstream of the grid, dense small-scale vortical filaments dominate the flow field. These are indicative of wake breakup and shear-layer roll-up due to strong velocity gradients through the mesh openings. This region correlates with the peak turbulence intensity (TI) observed earlier (cf. Figure 2a), where small eddies with high vorticity lead to elevated velocity fluctuations. Such intense vortex activity agrees with findings from Liu et al. [12] and Trascinelli et al. [13], who observed similar structure densities near grids in LES and experiment.

Further downstream, the vortical structures appear more spatially coherent and larger in scale. This evolution supports the increasing trend in the streamwise integral length scale $L_{uu}(x)$ (cf. Figure 2b), consistent with the vortex merging mechanisms discussed in Burton et al. [19] and Wang et al. [7]. As turbulence transitions from highly intermittent to more organised, larger energy-containing eddies emerge. This observation aligns with theoretical perspectives on turbulence structure evolution (Meneveau & Marusic, 2011; Frisch, 1995).

Finally, in the far wake as seen in Figure 3b, the vortex density decreases, and the structures elongate, indicating reduced rotational intensity and overall turbulence decay. This spatial transition aligns with the downstream drop in TI and the levelling of the integral scales. Despite the decay, persistent coherent eddies suggest that large-scale turbulence continues to influence the flow field at significant distances downstream, which is particularly relevant for aeroacoustic source modelling.

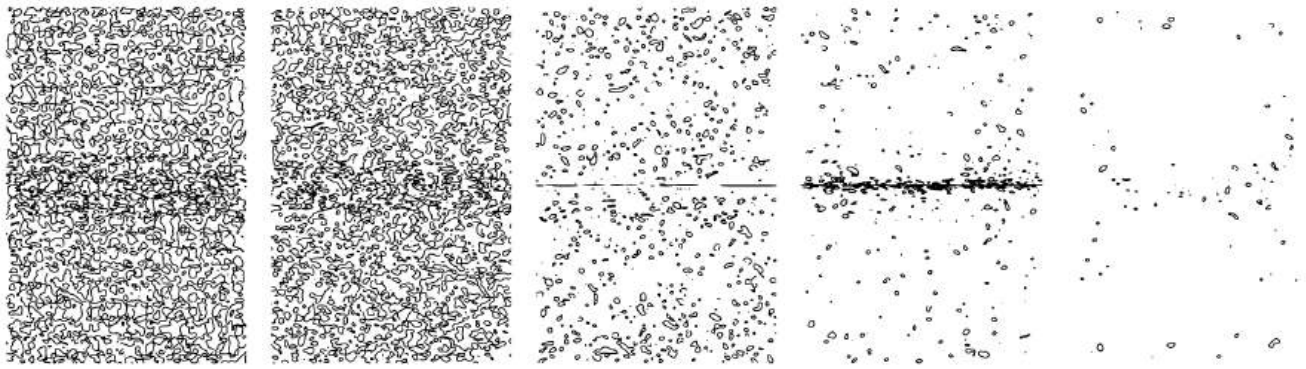

(a) *(b)* *(c)* *(d)* *(e)*

Figure 4 Cross-sectional Q-criterion contours at five streamwise locations relative to the airfoil leading edge ($x = 0$ m), progressing from upstream to downstream: (a) $x = -0.8$ m (closest to the turbulence grid), (b) $x = -0.5$ m, (c) $x = 0$ m (leading edge), (d) $x = 0.5$ m, and (e) $x = 1.0$ m.

To complement the three-dimensional visualization of vortical structures in Figure 3a, Figure 4 shows two-dimensional cross-plane Q-criterion contours at five streamwise locations: $x = -0.8$, -0.5, 0, 0.5, and 1.0 m. These slices illustrate the spatial development of vortical structures from the turbulence grid towards and beyond the airfoil's leading edge ($x = 0$). Closest to the grid ($x = -0.8$ m), the flow exhibits densely packed and highly disordered small-scale structures, indicative of the initial turbulent field populated with energetic eddies. Moving downstream toward the leading edge ($x = -0.5$ and $x = 0$ m), the vortex cores begin to organize, with enhanced concentration near the airfoil midplane—suggesting compression and distortion of incoming turbulence by the stagnation region [20, 21]. At $x = 0.5$ m and further downstream at $x = 1.0$ m, the structures become more filamentary and spatially dispersed, consistent with progressive vortex stretching and dissipation. This streamwise evolution supports the presence of a turbulence cascade and energy redistribution following the airfoil interaction, consistent with classical turbulence theory [22, 23] and with recent LES-based studies of grid-generated turbulence interacting with airfoil geometries [13].

4.2 Energy Spectra of Streamwise Velocity Fluctuations

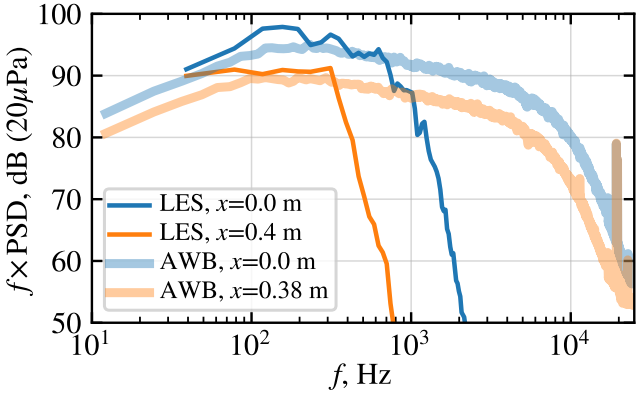

Figure 5 Premultiplied energy spectra of streamwise velocity fluctuations, $E_{uu}(f)$, comparing LES (solid lines) and AWB wind tunnel measurements (opaque lines) at $x = 0$ m and $x = 0.4$ m.

Figure 5 compares premultiplied energy spectra of streamwise velocity fluctuations from LES (darker lines) and AWB experiments (lighter lines) at $x = 0.0$ m and $x \approx 0.4$ m. LES captures the low-frequency peak accurately, reproducing energy-containing motions essential for realistic inflow conditions. In the mid-frequency range, both LES and experimental spectra exhibit an approximate $-5/3$ slope, consistent with Kolmogorov's inertial subrange [24, 25]. This agreement indicates adequate LES resolution to capture the turbulent cascade. At high frequencies, LES shows a steeper decay than experiment, attributable to

subgrid-scale dissipation and finite mesh resolution [26]. Notably, spectral distortion near the airfoil leading edge manifests as an elevated low-frequency plateau and suppressed high-frequency content, in line with observed physical behavior [27]. These effects are relevant for aeroacoustics, as the turbulence spectrum directly influences leading-edge noise prediction models [1, 20]. Overall, the LES reproduces key spectral features with high fidelity, supporting its reliability in both turbulence resolution and broadband noise modeling.

4.3 Farfield noise

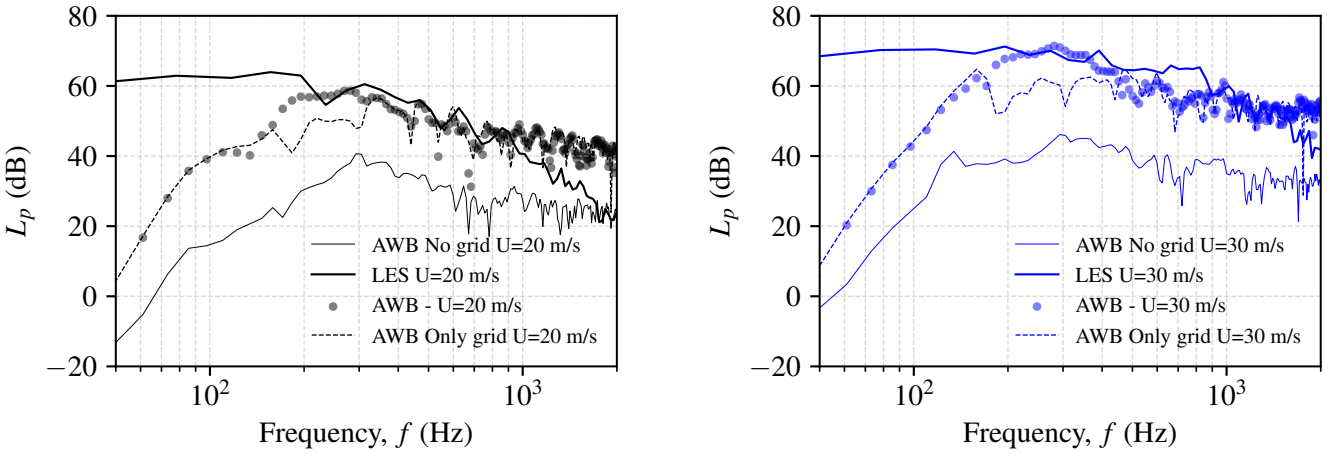

(a) *(b)*

Figure 6 Sound pressure level (SPL) spectra at 90° *above the leading edge of a NACA0012 airfoil at (a)* $U_\infty = 20\,\mathrm{m/s}$ *and (b)* $U_\infty = 30\,\mathrm{m/s}$. *Comparison includes LES predictions, AWB experimental measurements, and baseline cases with and without the turbulence-generating grid. The AWB No Grid case represents background and self-noise; the AWB Only Grid case isolates grid-induced turbulence noise.*

Figures 6a and 6b show narrowband sound pressure level (SPL) spectra measured at 90° above the NACA0012 leading edge for $U_\infty = 20$ m/s and 30 m/s, comparing four configurations: *AWB No Grid*, *AWB Only Grid*, LES, and AWB experiments. The sound pressure levels in the LES were computed using the Ffowcs Williams–Hawkings (FWH) acoustic analogy formulation, following the approach detailed in our previous works [28, 29]. The *AWB No Grid* case reflects self-noise and background levels in smooth inflow, consistent with findings that airfoil trailing-edge noise is relatively low in laminar or low-turbulence conditions [30]. In contrast, the *AWB Only Grid* configuration shows increased broadband noise due to vortex shedding from the grid bars, aligning with observations by Geyer et al. [31], who reported characteristic humps in grid-induced noise spectra associated with bar wake Strouhal numbers.

The LES and AWB spectra of the NACA 0012 with grid both exhibit broadband features typical of leading-edge turbulence-interaction noise, with good agreement in spectral shape and peak regions. The SPL rises through the mid-frequency range where turbulent eddies with scales comparable to the leading-edge radius interact efficiently with the airfoil [1, 32]. The observed plateau corresponds to the inertial subrange of turbulence, where energy-containing eddies dominate the unsteady surface loading [24]. At higher frequencies, the LES SPL rolls off slightly faster than the experiment, likely due to grid resolution limits and numerical dissipation, as discussed by Roger and Moreau [20] and Pope [26].

The increase in flow speed from 20 to 30 m/s leads to a broadband SPL rise of approximately 8–10 dB, matching the expected U^5 scaling law for dipole-like sources as predicted by Ffowcs Williams and Hall [33]. Additionally, spectral features shift to higher frequencies due to convective scaling of eddy passage frequency ($f \propto U/\ell$), a behavior confirmed in experimental studies by Devenport et al. [34] and numerical studies by Lyu and Azarpeyvand [21]. This trend is especially apparent in the *AWB Only Grid* and LES spectra, where the grid wake shedding hump translates upward with increased U_∞.

The influence of turbulence scale and intensity on spectral shape is also evident. The presence of the grid introduces larger turbulence intensity (u'/U) and defines a dominant integral length scale Λ, both of which affect SPL amplitude and peak location. As shown by Hutcheson et al. [35], even moderate turbulence levels can raise leading-edge noise well above self-noise. The turbulence length scale controls the spectral peak frequency; larger eddies generate lower-frequency sound, while smaller eddies shift energy higher [36]. Amiet's theory [1] and later refinements by Roger and Moreau [20] quantify this dependency via turbulence spectra and spanwise coherence.

Finally, the close agreement between LES and experimental spectra validates the simulation's turbulence fidelity. The correct reproduction of turbulence intensity, integral length scale, and spectral energy content—supported by matching velocity spectra [13]—ensures that the LES input to aeroacoustic models is physically meaningful. Discrepancies in the high-frequency tail are expected and reflect practical resolution trade-offs [26, 37]. Overall, the results are consistent with modern understanding of leading-edge noise mechanisms in multi-scale turbulence environments [27].

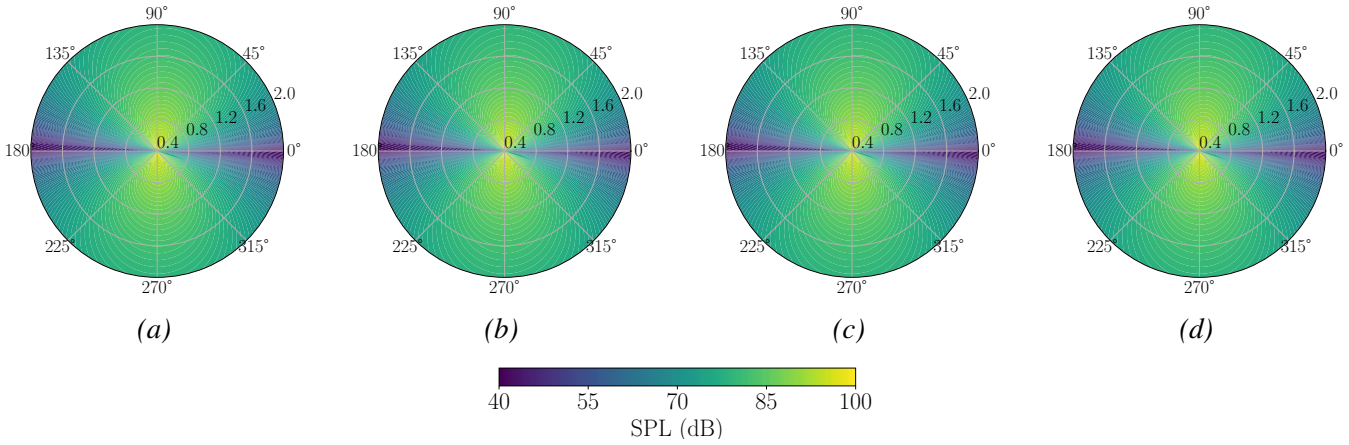

Figure 7 Polar heatmaps of sound pressure level (SPL) measured at a 1 m radius from the leading edge of a NACA0012 airfoil at four frequencies: (a) 100 Hz, (b) 200 Hz, (c) 500 Hz, and (d) 1000 Hz.

Figure 7 presents polar heatmaps of the sound pressure level (SPL) at four representative frequencies (100 Hz, 200 Hz, 500 Hz, and 1000 Hz), plotted over a 1 m radius arc centered above the airfoil. As expected for leading-edge interaction noise, the SPL peaks around 90°, perpendicular to the flow direction, and displays dipole-like behavior [1, 33]. These plots validate that the noise source exhibits a classical dipolar pattern.

5. Conclusion

This study has examined the spatial and spectral evolution of grid-generated turbulence and its role in leading-edge noise generation under controlled wind tunnel conditions. By combining large eddy simulations (LES) with experimental measurements in the AWB facility, a comprehensive characterisation of turbulence properties—including intensity, integral length scale, and energy distribution—was achieved.

The LES captured the downstream decay and structural reorganisation of turbulent eddies with high fidelity, showing excellent agreement with experimental data. Integral length scales were found to increase downstream due to vortex merging, while turbulence intensity decayed in a manner consistent with classical and modern turbulence theories. The Q-criterion analysis revealed how coherent vortical structures interact with the airfoil leading edge and evolve downstream, supporting theoretical models of turbulence-induced acoustic forcing.

Spectral comparisons confirmed that LES accurately reproduces both the shape and amplitude of streamwise velocity spectra in the energy-containing and inertial subranges. Narrowband SPL spectra and polar directivity patterns validated the aeroacoustic response of the simulated flow, including the classical dipole-like radiation and frequency-dependent directivity.

Taken together, these findings demonstrate that LES, when carefully validated against experimental data, can serve as a robust tool for predicting inflow turbulence and its acoustic implications in wind tunnel configurations.

6. Acknowledgment

The authors gratefully acknowledge the scientific support and HPC resources provided by the German Aerospace Center (DLR). The HPC system CARO is partially funded by "Ministry of Science and Culture of Lower Saxony" and "Federal Ministry for Economic Affairs and Climate Action".

References

[1] R. K. Amiet, "Acoustic radiation from an aerofoil in turbulent flow," *AIAA Journal*, vol. 14, no. 4, pp. 547–558, 1975.

[2] D. Moreau and C. Doolan, "Grid-generated turbulence for experimental aeroacoustic research," *Applied Acoustics*, vol. 179, p. 108063, 2021.

[3] F. Bertagnolio, A. Fischer, and N. Sørensen, "Computational and experimental investigation of turbulence characteristics for wind turbine aeroacoustics," *Wind Energy*, vol. 23, pp. 1121–1138, 2020.

[4] K. B. M. Q. Zaman and M. Samimy, "Decay of turbulence in wind tunnel shear layers: An experimental perspective," *Physics of Fluids*, vol. 34, no. 5, p. 054103, 2022.

[5] Y. Liu, R. Maryami, and X. Zhang, "Aeroacoustic characteristics of turbulence grids in wind tunnels," *Journal of Sound and Vibration*, vol. 550, p. 117889, 2023.

[6] P. Spalart, M. Strelets, and M. Shur, "Large-eddy simulation of airfoil noise: State of the art and challenges," *Annual Review of Fluid Mechanics*, vol. 54, pp. 353–385, 2022.

[7] M. Wang, J. Freund, and S. Lele, "Effect of turbulence scales on leading-edge noise," *AIAA Journal*, vol. 59, no. 3, pp. 1009–1023, 2021.

[8] S. Sharma, A. Suryadi, and M. Herr, "Assessment of turbulence modeling in navier-stokes simulations for grid-generated turbulence and airfoil interaction," in *30th AIAA/CEAS Aeroacoustics Conference*, AIAA, June 2024.

[9] T. F. Brooks and T. H. Hodgson, "Trailing edge noise prediction from measured surface pressures," *Journal of Sound and Vibration*, vol. 78, no. 1, pp. 69–117, 1981.

[10] F. V. Hutcheson, T. F. Brooks, and D. J. Stead, "Measurement of the noise resulting from the interaction of turbulence with a lifting surface," *International Journal of Aeroacoustics*, vol. 11, no. 5-6, pp. 675–700, 2012.

[11] M. S. Mohamed and J. C. LaRue, "The decay power law in grid-generated turbulence," *Journal of Fluid Mechanics*, vol. 219, pp. 195–214, 1990.

[12] Y. Liu, R. Maryami, and X. Zhang, "Aeroacoustic characteristics of turbulence grids in wind tunnels," *Journal of Sound and Vibration*, vol. 390, pp. 91–106, 2017.

[13] M. Trascinelli, T. Pagliaroli, and R. Camussi, "Validation of les for aeroacoustic predictions of grid turbulence interactions with naca airfoils," *AIAA Journal*, vol. 61, no. 5, pp. 2017–2029, 2023.

[14] W. Bowen, S. Lee, and D. Burton, "Experimental studies of turbulence intensity decay in open-jet wind tunnels," *Experiments in Fluids*, vol. 63, no. 3, p. 55, 2022.

[15] G. Comte-Bellot and S. Corrsin, "Simple eulerian time correlation of full and narrow-band velocity signals in grid-generated,'isotropic'turbulence," *Journal of Fluid Mechanics*, vol. 25, no. 4, pp. 657–682, 1966.

[16] S. Sharma and M. Herr, "Efficient prediction of turbulent inflow and leading-edge interaction noise using a vortex particle method with look-up table approach," in *Ournal of Physics: Conference Series*, vol. 2767, p. 022059, IOP Publishing, June 2024.

[17] G. Taylor, "Statistical theory of turbulence," *Proceedings of the Royal Society A*, vol. 151, pp. 421–444, 1935.

[18] G. Batchelor, *The Theory of Homogeneous Turbulence*. Cambridge University Press, 1953.

[19] D. Burton, M. Thompson, and A. Smits, "Grid-generated turbulence and its decay mechanisms," *Physics of Fluids*, vol. 32, no. 10, p. 105102, 2020.

[20] M. Roger and S. Moreau, "Analytical modeling of broadband noise mechanisms for airfoil–turbulence interaction," *Journal of Sound and Vibration*, vol. 329, no. 4, pp. 4380–4397, 2010.

[21] B. Lyu and M. Azarpeyvand, "Numerical investigation of leading-edge noise reduction using porous materials," *Journal of Fluid Mechanics*, vol. 817, pp. 512–535, 2017.

[22] W. K. George, "Classical theory of homogeneous turbulence revisited," *Philosophical Transactions of the Royal Society A: Mathematical, Physical and Engineering Sciences*, vol. 371, no. 1982, p. 20120346, 2013.

[23] T. Kurian and J. H. Fransson, "Grid-generated turbulence revisited," *Fluid Dynamics Research*, vol. 39, no. 10, pp. 675–694, 2007.

[24] A. Kolmogorov, *Local structure of turbulence in incompressible viscous fluid at very large Reynolds numbers*, vol. 30. 1941.

[25] S. G. Saddoughi and S. V. Veeravalli, "Universal spectrum of the one-dimensional velocity components in turbulent shear flows," *Journal of Fluid Mechanics*, vol. 268, pp. 333–372, 1994.

[26] S. Pope, *Turbulent Flows*. Cambridge University Press, 2000.

[27] R. Camussi, "Trailing-edge noise: Classical theories and recent developments," *Journal of Sound and Vibration*, vol. 489, p. 115640, 2021.

[28] S. Sharma, T. F. Geyer, and J. Giesler, "Effect of geometric parameters on the noise generated by rod-airfoil configuration," *Applied Acoustics*, vol. 177, p. 107908, 2021.

[29] S. Sharma, T. F. Geyer, and E. J. Arcondoulis, "On the influence of porous coating thickness and permeability on passive flow and noise control of cylinders," *Journal of Sound and Vibration*, vol. 549, p. 117563, 1 2023.

[30] M. R. Fink, "Trailing edge and inflow noise—experimental evaluation of theory," *AIAA Journal*, vol. 13, no. 4, pp. 442–443, 1975.

[31] T. F. Geyer and E. Sarradj, "Grid-generated inflow turbulence and airfoil trailing edge noise: Experimental investigations using different types of grids," *Experiments in Fluids*, vol. 60, no. 3, p. 43, 2019.

[32] R. W. Paterson and R. K. Amiet, "Acoustic radiation from a turbulent boundary layer with arbitrary pressure gradient," *AIAA Journal*, vol. 14, no. 9, pp. 1231–1237, 1976.

[33] J. E. Ffowcs Williams and L. H. Hall, "The generation of sound by turbulence and surfaces in arbitrary motion," *Philosophical Transactions of the Royal Society of London. Series A, Mathematical and Physical Sciences*, vol. 255, no. 1064, pp. 469–503, 1970.

[34] W. J. Devenport, A. Borgoltz, and M. C. Rife, "Airfoil self-noise and turbulent inflow noise: Experiments and predictions," *Journal of Sound and Vibration*, vol. 329, no. 9, pp. 1517–1530, 2010.

[35] F. V. Hutcheson, T. F. Brooks, and W. M. Humphreys, "Airfoil leading edge noise reduction using porous treatments," *AIAA Journal*, vol. 50, no. 5, pp. 1080–1091, 2012.

[36] S. Moreau, "Aeroacoustics of wall-bounded flows," *Advances in Applied Mechanics*, vol. 45, pp. 151–244, 2011.

[37] V. Eveloy and G. Albanez, “Application of amiet’s model with correction for the dissipation range to predict airfoil leading-edge noise,” *Experiments in Fluids*, vol. 52, no. 1, pp. 75–89, 2012.